Turbulence and Heat Release Rate Network Structure in Hydrogen-enriched Combustion

Marcin Rywik[a,*], Praveen Kasthuri[b], Isaac Boxx[c], Ianko Chterev[c], Wolfgang Polifke[a], R. I. Sujith[b]

[a] *Department of Engineering Physics and Computation, School of Engineering & Design, Technical University of Munich, 85748 Garching, Germany*
[b] *Department of Aerospace Engineering, Indian Institute of Technology Madras, Chennai - 600036, India*
[c] *Institute for Combustion Technology, German Aerospace Centre (DLR), 70569 Stuttgart, Germany*

Abstract

Complex network theory is used to analyze the spatiotemporal dynamics of the PRECCINSTA swirl burner, operating on hydrogen-methane fuel blends. At a power setting of 15 kW with equivalence ratio of 0.8 and hydrogen fuel fraction (HFF) ranging from 0% to 80%, period-1 and period-2 limit cycle oscillations as well as chaotic oscillations were observed. A turbulence network was constructed from the vorticity data obtained with particle image velocimetry. In addition, a heat release rate (HRR) correlation network was constructed from chemiluminescence images. Although the two networks concern a common thermoacoustic system, both exhibit significant differences: the turbulence network displays power law degree distribution, maintains small world property for all HFFs and is scale-free only in the absence of hydrogen enrichment. The HRR correlation network does not feature these properties, but hints at an asymmetric coupling between the heat release rate and the acoustic pressure for all HFFs. Furthermore, the HRR network is responsive to changes in HFF and the corresponding shifts in the dynamical state as well as in the root-mean-square of acoustic pressure. On the contrary, the turbulence network displays no such sensitivity and its properties are almost constant in the upper HFF range. It exhibits stationary hub structures for all the fuel blends tested, whereas the HRR correlation network is hub-free.

Keywords: Thermoacoustic instability; hydrogen combustion; complex networks

1. Introduction

Thermoacoustic instabilities are an important design challenge for modern combustors used in land-based power generators, aeronautical and rocket propulsion systems as well as industrial boilers [1]. According to Rayleigh, thermoacoustic instability can occur when the unstable heat release rate is mostly in-phase with acoustic pressure [2]. If this condition is satisfied, acoustic pressure oscillations may grow to a high-amplitude limit cycle. Today, ecological considerations advocate reduction of emissions and enforce operation in lean conditions, which exacerbates thermoacoustic instability concerns.

In combustion science, hydrogen is viewed as a potential answer to restrictive pollution regulations and the need for carbon-neutral, on-demand power generation [3]. However, as the properties of hydrogen differ from those of conventional hydrocarbon fuels, its introduction is not straightforward [4]. Therefore, fuel blends of hydrogen with hydrocarbons are being considered as an intermediate solution. Such fuel blends display various thermoacoustic instabilities, depending on the operating conditions and blend proportions [5]. Instability levels cannot be related in a straightforward manner to hydrogen content. Indeed, injection of small amounts of hydrogen as pilot fuel was used as a means of passive control of instabilities [6].

The design of instability suppression devices is often costly, requiring a trial and error approach due to the complexity of the thermoacoustic system. Promising results were achieved recently by identifying and targeting regions responsible for maintaining a thermoacoustic instability by means of complex networks [7]. Complex networks theory is an emerging field of science used to analyze the temporal and spatiotemporal behavior of diverse systems [8]. The topic has become increasingly popular, with a variety of approaches reported in non-reacting [9] and reacting [10] fluid flows. Applications include velocity correlation networks in hemodynamics [11], which identify geometrical features of carotid bifurcation that deteriorate spatiotemporal similarity. In another study, a robust reduced order model of high-dimensional nonlinear vortical interactions was obtained by performing a network community collapse [12]. Complex networks were combined with machine learning for early detection of transition by amplifying subtle changes associated with an in-phase state [13]. Additionally, complex networks were used to investigate the distribution of acoustic power within a combustor [14], revealing the regions most crucial for thermoacoustic driving.

In the present study we concentrate on turbulence networks and correlation networks in the PRECCINSTA combustor for various levels of hydrogen fuel enrichment. Both network approaches were applied in fluid mechanics and thermoacoustic fields previously. Turbulence networks revealed information on patterns within vortical structures [14, 15], while correlation networks were constructed to assess the state and critical regions of the flow field. Two-point correlation networks of velocity [16] and kinetic energy time histories [17] were previously formulated. This time, instead of investigating correlation between quantities related to velocity, the reactive field was the focus, resulting in a heat release rate correlation network, which only recently has been introduced in [18]. Together with the turbulence network, we had two distinct networks to analyze, constructed from the same experimental data set. This was contrary to previous investigations which focused only on one of those exclusively. The objective of this study is to investigate whether the vortical structures and heat release rate field produce networks of similar properties or complement each other with additional information about the analyzed system.

2. Experimental setup

The dataset utilized in this study originated from measurements conducted on the PRECCINSTA configuration swirl burner, which is a widely studied technically premixed gas turbine model combustor [19, 20]. The combustor in Fig. 1 consists of a cylindrical plenum, a swirl generator, a combustion chamber with a 85×85 mm^2 cross-section and a 114 mm height as well as an exit nozzle with an exhaust duct. Visual access was provided by quartz glass side walls and acoustic pressure measurements were acquired at a rate of 100 kHz, using a condenser microphone positioned at a distance of 20 mm from the dump plane. The velocity field (u, v, w) was recorded at 10 kHz through stereoscopic particle image velocimetry (PIV), resulting in a 640×800 pixel resolution in -42.5 mm $<$ x $<$ 42.5 mm and 0 mm $<$ y $<$ 50

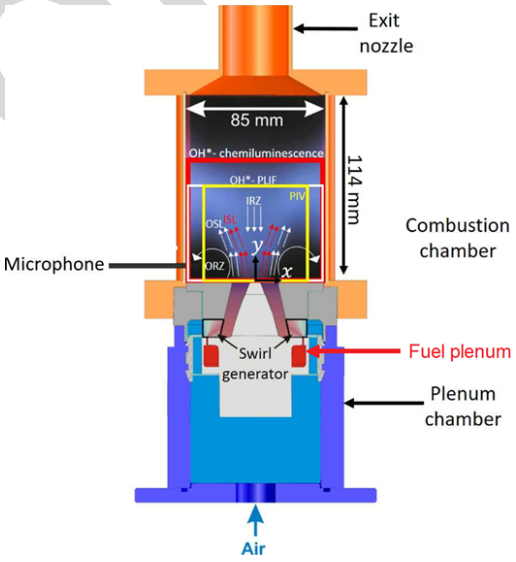

Fig. 1: An adapted overview of the experimental setup [5].

mm ranges. Line of sight integrated chemiluminescence from self-excited OH* radical was captured at 10 kHz over 0.82 seconds. The resultant 8192 images had a resolution of 512 × 512 pixels and were used for heat release rate field analysis.

The experiments were conducted for configurations involving multiple thermal loads P and equivalence ratios ϕ while varying hydrogen enrichment, recently presented in [5]. The hydrogen fuel fraction (HFF) of the hydrogen-methane mixture was defined as,

$$HFF = \dot{V}_{H_2}/(\dot{V}_{H_2} + \dot{V}_{CH_4}) \tag{1}$$

$\dot{V}$ denotes standard volume flow rates of hydrogen (H_2) and methane (CH_4). The HFF was swept from 0%-80%, in steps of 10%. The measurements were a part of a larger research effort, focusing on the effect of hydrogen use in gas turbine powerplants. There, the combustor is a single sub-component, designed to operate at a specific thermal load. Thus, through the HFF sweep P and ϕ were held constant, while flow rates were being adjusted. A more detailed description of the experimental setup is available in [5].

3. Network construction

A network consists of nodes connected by links, forming an interconnected structure. Complex networks theory aims to detect fundamental behavior patterns. Instead of considering each node separately, the complex network framework focuses on the resultant interaction between them. To assess this interaction, a multitude of complex network measures such as degree, degree distribution, betweenness centrality, and clustering coefficient are commonly utilized [8]. In our case, the links connecting any two nodes are assigned weights as opposed to mere binary connections, resulting in a weighted network. An adjacency matrix A_{ij} contains all the necessary data for a network to be analyzed or visualized. Each element A_{ij} of the adjacency matrix denotes the weight of a connection between nodes i and j. The exact definitions behind the terms 'node' and 'link' as well as the rules for determining a weight depend on the type of the network constructed. In a continuous system nodes are often created by a spatial discretization, e.g. using grid points as nodes, as is the case here.

This study makes use of two well-established networks - a turbulence network [21] and a correlation network [16], namely a heat release rate (HRR) correlation network. In the following subsections, the specific construction procedure for each of the networks is briefly described.

3.1. Turbulence network

The turbulence network aims to capture the relation between vortical structures in the flow domain and identify the locations most influenced by them. It was shown to be able to distinguish between different dynamical states and highlight structures crucial to maintaining thermoacoustic instability [7]. This network quantifies how much velocity is induced at each grid cell (node i) due to the vorticity present at another grid cell (node j). All the possible pairings in the considered spatial domain are eligible for the calculation and the induced velocity is computed from the PIV data, following the Biot-Savart law [21]:

$$u_{i\to j} = \frac{|\omega(x_i,t)\Delta x\Delta y|}{2\pi|x_i - x_j|}, \tag{2}$$

where $u_{i\to j}$ is the velocity induced at position x_j due to vorticity ω present at x_i, given the grid resolution Δx and Δy in x and y direction respectively. The value of Eq. (2) is finite only if i and j are different, which is reflected in the next step. Following [21], the adjacency matrix A_t of a turbulence network is defined as

$$A_{t_{ij}}(t) = \begin{cases} \frac{1}{2}(u_{i\to j} + u_{j\to i}) & \text{, if } i \neq j \\ 0 & \text{, if } i = j. \end{cases} \tag{3}$$

The resultant network is undirected and includes no self-loops, as the adjacency matrix A_t is symmetric and the diagonal entries are all zeros, respectively. The adjacency matrix A_t was constructed using vorticity evaluated from the PIV data after cropping off the edges to remove the measurement artifacts at the window boundaries. Note, that the turbulence network is a time-varying network.

3.2. Heat release rate correlation network

An HRR correlation network captures the coherence of the reactive field, using correlation measures [18]. To construct it, line-of-sight integrated OH* chemiluminescence was used as an HRR proxy. Next, Pearson correlation was selected as it is the most sensitive and yet the least computationally expensive measure. A link between each pair of nodes (grid point locations i and j) is established with a strength corresponding to the Pearson correlation value R_{ij} between HRR histories $\dot{q}'(t)_i$ and $\dot{q}'(t)_j$ observed at those locations. The R_{ij} value is calculated over 50 $\Delta t = 0.1$ ms time steps: the current one and 49 past ones. 50 time steps were an optimal time window as it then commensurated with a few acoustic cycles, preventing too noisy results or too aggressive time-averaging [22]. In our case, depending on HFF we cover up to three cycles of the dominant frequency (Fig. 2), which we empirically verified as a suitable choice. The adjacency matrix of an HRR correlation network is defined as

$$A_{HRR_{ij}}(t) = \begin{cases} R_{ij}(t) & \text{, if } i \neq j \\ 0 & \text{, if } i = j. \end{cases} \tag{4}$$

As Pearson correlation is a commutative operation, it automatically results in HHR correlation network being undirected and without self-loops, similarly to

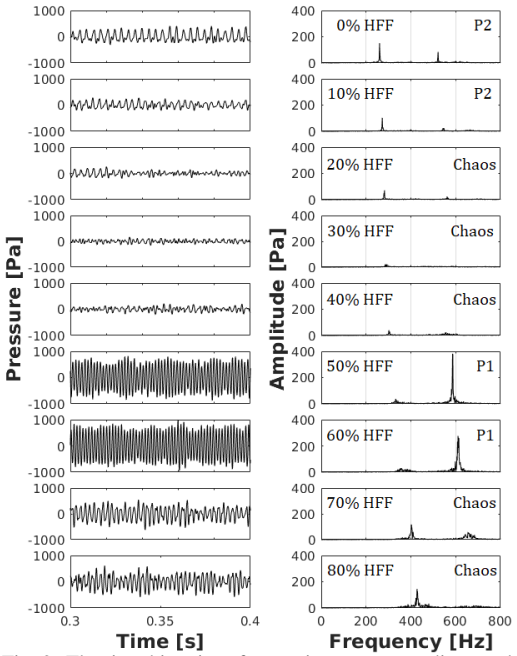

Fig. 2: The time histories of acoustic pressure readings and the corresponding amplitude spectra for HFFs between 0% to 80%.

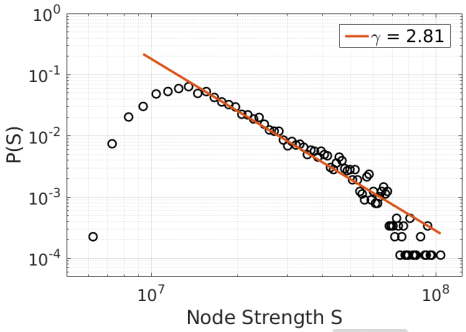

Fig. 3: A log-log plot of the degree probability distribution of a turbulence network with a linear fit of slope $-\gamma$. The distribution follows a power law $P(S) \sim S^{-\gamma}$, characteristic for the complex network framework [8].

the turbulence network. Although correlation is a time-averaged measure, the resultant network is time-varying as its structure is recalculated at every time step, adjusting the 50 ms time window used for correlation estimate.

4. Results

In this study, the spatiotemporal dynamics at different HFF levels was characterized using turbulence and HRR correlation networks. As mentioned in Section 2., measurements for multiple combustor operating condition with varying HFF were available. We have decided to focus on a single HFF sweep for thermal load of 15 kW and equivalence ratio of 0.8. This configuration presented the most dynamically varied behavior and non-monotonic relation between the HFF and the root-mean-square (RMS) of acoustic pressure p'_{rms}. As such, it provided a suitably challenging test for the complex network framework.

4.1. Data overview

For the selected case ($P = 15$ kW, $\phi = 0.8$) as HFF is varied from 0% to 80%, the acquired combustion data displayed multiple dynamical states. They ranged from chaos, intermittency to period-1 (P1) and period-2 (P2) oscillations [5]. In the absence of hydrogen or for a low HFF, the selected case exhibited a low amplitude P2 instability with two distinct frequencies registered. Shifting towards greater hydrogen content, stable combustion characterized by aperiodic chaotic oscillations was obtained. Increasing the HFF further, the system switched to a high amplitude P1 instability with a single dominant frequency. Finally, for the most hydrogen-rich fuel blends the combustion returned to a chaotic state, yet with significantly greater p'_{rms} readings compared to the stable operation previously encountered.

4.2. Turbulence networks

A turbulence network – constructed as described in Section 3.1. – establishes to which extent a given location is affected by vortices spread over the entire spatial domain. For the constructed turbulence network, the degree distribution and its power law exponent as well as the hub structures were the most interesting features and are described in the following.

4.2.1. Degree distribution

The degree distribution is a probability distribution of the sum of links, here weighted, that a node is connected to. Complex network theory suggests that the degree distribution of many real-world phenomena does not follow a normal, but instead a power law distribution, with its exponent having a significant importance in the network structure.

We analyzed the probability distribution of node strength S of the turbulence network across the 0% to 80% HFF range and the corresponding dynamical states. The networks adhered to the power law for all values of HFF and time steps analyzed. Figure 3 exhibits but one example with an exponent γ equal to 2.81. One might wonder why a linear fit is implemented, although the tails of the distribution are not well modeled by it. Indeed, those deviations are expected in the complex network framework. The RHS tail is affected by a linear binning phenomenon as a discrete integer count unit is used. Additionally, the number of possible connections is restricted by the PIV resolution. Therefore, the strongest nodes have

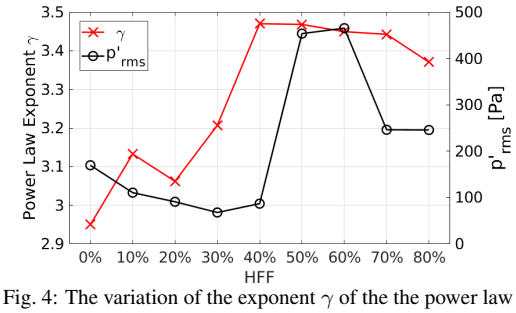

Fig. 4: The variation of the exponent γ of the the power law fit of the degree distribution, along with the corresponding p'_{rms} for HFFs from 0% to 80%.

limited linking opportunities, scarcer than theoretically predicted by the power law. Hence, the RHS tail of the distribution is overestimated by the linear fit, referred to as a 'high degree cut-off'. On the other hand, the LHS tail of the distribution is tapered due to a 'low degree saturation'. This behavior is modeled via an attractiveness node measure, which modifies the power law in the lower limit [8]. In our case, one of the reasons for the nonzero attractiveness could be associated with each node always having some velocity induced due to even weak vorticity levels in the immediate vicinity, due to Eq. (2) always resulting in a positive value.

Complex network theory predicts that networks exhibiting a power law distribution should develop so called 'hubs'. Hubs – i.e. nodes with the greatest number of connections, which cannot be accounted for by random graph theory – are a crucial element to the integrity and connectivity of the network. The behavior of networks with hubs is robust against perturbations applied to randomly chosen nodes, but highly susceptible when hubs are targeted [8].

Similar power law behavior was observed by Murayama et al. [15] and Krishnan et al. [7]. However, both these studies did not test the effect of hydrogen enrichment. Moreover, the latter was performed on a bluff-body stabilized burner, rather than a swirl one. Despite those differences, all the constructed networks retained and exhibited power law, suggesting it could be a universal feature of vortical structures in turbulent combustors. Analogously, the power law distribution is widely accepted in turbulence as the Kolmogorov's 5/3 energy spectrum and the resultant network properties could be its consequence.

4.2.2. Power law exponent of the degree distribution

As previously mentioned, the power law exponent γ conveys important knowledge about the network, e.g. concerning information propagation and hub sizes. The changes of the value of the exponent γ with increasing HFF did not seem to exhibit any particular sensitivity to changes in dynamical state and p'_{rms}. It increased from approximately 2.95 to 3.45 with HFF reaching up to 40%, after which it relatively saturated. The exponent never increased above the value of 4. Power law networks with $\gamma<4$, can be safely considered 'small world' networks [8]. The small world property refers to a network having shortcut connections between distant nodes. As a result, the average path lengths, i.e. the number of steps along the links to move from one node to another, is greatly reduced. The interpretation of the small world property is that information propagates quickly through the network and the lag associated with its propagation scales weakly with the network size. Following that, local perturbations are expected to have a rapid and increased impact on the global behavior.

In networks with γ values below 3, we encounter a stronger version of that property - 'ultra small world' [8]. The average path length is then even less affected by the size of the network. Additionally, those networks display a 'scale-free' feature, i.e., with increasing number of nodes the standard deviation of the degree distribution diverges. It in fact renders the concept of the mean degree meaningless. In other words, the mean degree cannot be used to estimate the degree of the smallest nodes and the most connected hubs. The connectivity of such networks becomes increasingly reliant on the hubs as they become more dominant. It was found that only in the absence of hydrogen enrichment was the turbulence network scale-free. Possibly, the introduction of hydrogen brings out a heterogeneity in the combustion dynamics since hydrogen is combusted rapidly within smaller length scales. This could be the reason behind the absence of ultra small world property for hydrogen blends.

Contrary to the previous study [7], the exponent γ could not be directly related to dynamical states. No unambiguous trends were observed when the state switched between instability and chaotic oscillations, as well as when the p'_{rms} value altered, see Fig. 4. The results here and in the subsequent subsection suggest that the exact magnitude of γ is rather linked to the hub evolution. The value of γ and hub structures ceased to change past the 40% hydrogen content and remained approximately constant. Similarly, past 40% HFF a diminished variability of HRR within the inner recirculation zone in comparison to the shear layer was observed. Given a varied selection of dynamical states tested, the turbulence network did not experience major changes, even when p'_{rms} was shifted significantly by a single HFF step.

4.2.3. Hub structures

The power law distribution indicates that the turbulence network exhibits hubs. The hubs are the most connected nodes, responsible for the integrity of the network and fast information propagation. In this study hubs were classified as the top 0.5% of the strongest nodes, i.e. nodes for which S is extremely high. Figure 5 depicts the change in time-averaged position of the hubs with increasing HFF. Due to Eq. 2, the strongest nodes in the turbulent network lie in the regions of intense vorticity. Hence,

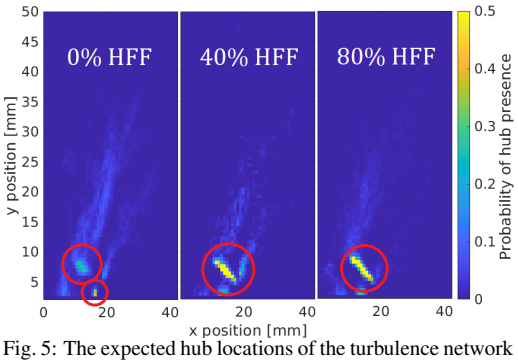

Fig. 5: The expected hub locations of the turbulence network in the RHS half-plane of the combustor, for selected HFFs.

the inner and outer shear layers are highlighted, indicating at least a temporary presence of hubs. At low HFF there exists a pair, consisting of a primary and a secondary hub structure, at each side of the shear layer. Their locations match the regions of vortex shedding, especially off the inner side. However, for greater HFF values the hub structure begins to span across the whole shear layer rather than highlighting only its edges. With increasing hydrogen content, the pair coalesces at 40% HFF and ceases to alter throughout. Additionally, the effect of hub convection is diminished as indicated by the vanishing elongated signature for higher hydrogen contents. This behavior corresponds to the saturation of the power law exponent γ occurring analogously at 40% HFF. Most notably, the expected position of the hub does not change significantly with fuel compositions. The PIV data shows that the swirl branches switch to a wider shape beyond 40% HFF. The vortices on both sides of the shear layer are hence pushed apart. The increased distance between them weakens their interaction and reduces the sensitivity of the network to positional changes of the said vortices, potentially accounting for the γ value saturation and no further shifts in the hub structure.

In fact, the connectivity of the networks with a power law degree distribution relies heavily on the hub structures [8]. Suppressing the hubs of a turbulence network was previously shown to inhibit thermoacoustic instability [7]. Estimation of the hub location facilitates the design of such an effective targeted suppression. However, its implementation is most convenient when the hub location is always the same. As shown in Fig. 5, not only did the addition of hydrogen preserve the hub structures of the network, but the hub location was mostly stationary in time and its expected position did not change with increasing HFF. Subsequently, hub-disrupting suppression systems should be in principle applicable throughout the whole range of hydrogen enrichment, with no need for any major adjustments, reducing the development resources required.

4.3. Heat release rate correlation network

The HRR correlation network is a weighted network, with the weights determining the strength of the interactions between two locations in the spatial domain, as determined by Eq. 4. As the network aims to capture the level of coherence of HRR oscillations, sensitivity to dynamical state and temporal p'_{rms} values were investigated.

4.3.1. Dynamical sensitivity

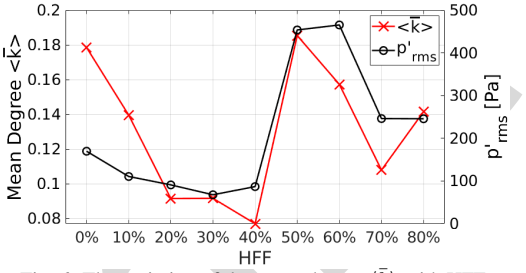

Fig. 6: The variation of the mean degree $\langle \bar{k} \rangle$ with HFF.

When thermoacoustic instabilities were present, some extent of HRR field synchronization was expected. This was visualized by the time-averaged mean degree $\langle \bar{k} \rangle$, which quantifies the average weighted number of links a node in the network is connected to and here, the term 'mean' is used in a spatial sense. Examining Fig. 6, it was observed that the occurrence of a thermoacoustic instability is accompanied by the increased HRR field synchronization as indicated by the mean degree $\langle \bar{k} \rangle$ and as expected by the paradigm. Indeed, $\langle \bar{k} \rangle$ attained high values for both P2 and P1 oscillations cases, e.g. at HFFs of 0% and 50% respectively. In contrast, the $\langle \bar{k} \rangle$ values were lower for operating conditions displaying chaotic behavior - HFF of 20% to 40% and 70% to 80%. The mean degree measure $\langle \bar{k} \rangle$ was sensitive to shifts in dynamical state, but matched the changes in p'_{rms} only qualitatively. For both cases exhibiting thermoacoustic instability (0% and 50% HFF) values of $\langle \bar{k} \rangle$ were comparable, despite a substantial difference in the value of acoustic pressure. High synchronization of the HRR field seemed to be a necessary condition for a thermoacoustic instability. Yet, it was insufficient to explain the expected p'_{rms}, with e.g. damping being an amplitude suppressing factor, not considered by the network.

4.3.2. Temporal sensitivity to RMS of acoustic pressure

In Section 4.3.1., only the time-averaged results for each HFF were presented. Here, we focus on the temporal changes in the network, providing insight into the evolution of the HRR field.

Figure 7 presents the temporal evolution of the network. With correlation being an inherently a time-averaged measure, the p'_{rms} value was chosen for

Table 1: Cross-correlation results between the mean degree $\langle k \rangle$ and RMS of acoustic pressure p'_{rms} for different HFFs.

Hydrogen Content	Cross-correlation Value R	Optimum Lag [1 ms]
0%	0.81	2
10%	0.63	1
20%	0.85	1
30%	0.71	1
40%	0.60	1
50%	0.76	1
60%	0.70	1
70%	0.60	1
80%	0.62	1

comparison. The p'_{rms} estimation was done over fifty current and previous time steps ($\Delta t = 0.1$ ms) to ensure the same number of regressors as for the HRR correlation calculations. Both measurements had a noticeable dependence, namely they were positively correlated. In contrast with the time-averaged measures, the instantaneous networks seemed to behave more consistently in terms of reflecting the p'_{rms} values. The mean degree measure $\langle k \rangle$ of the HRR network varied significantly, including differences reaching close to an order of magnitude.

The time-histories continued to be positively correlated throughout the whole HFF range tested, with measured values always greater than 0.6 as noted in Table 1. Cross-correlation was utilized, not only to quantify the dependence but also to assess the order in which the signals were changing. For all test cases, the optimum time lag resulting in the greatest correlation value was always positive. This meant the mean degree $\langle k \rangle$ of the network and inherently the HRR field were shifting earlier, at least on average, than the p'_{rms} trace. This is in agreement with a recent finding, that the synchronization between acoustic pressure p' and heat release rate $\dot{q}'$, despite being bidirectional, is asymmetric with the latter influencing the former more strongly than vice versa [23, 24].

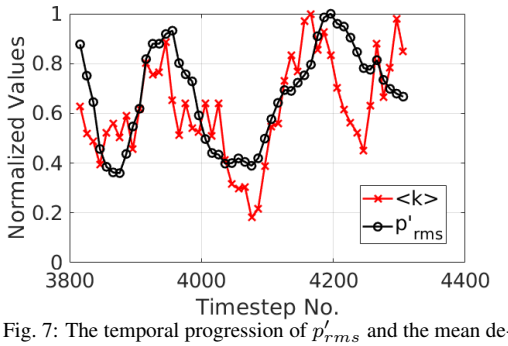

Fig. 7: The temporal progression of p'_{rms} and the mean degree $\langle k \rangle$ of an HRR network over approximately 20 pressure cycles for 80% HFF.

4.3.3. OH-chemiluminescence as an HRR proxy*

Due to the experimental nature of the data, changes in local equivalence ratio could not be excluded. Thus, we could expect certain uncertainties by representing HRR with OH*-chemiluminescence. Despite this, we believed the latter is a suitable proxy in the PRECCINSTA burner for this study. The HRR network framework aimed to investigate global patterns and relative changes within the whole domain over a few cycles. The HRR network calculation relied on a correlation measure, which is inherently a time-averaged quantity, reducing the influence of instantaneous uncertainties. Meier et al. [19] has shown that when phase-averaged with respect to the thermoacoustic pulsation, OH* chemiluminescence closely tracks the pressure fluctuation. Although the amplitude of HRR fluctuations is not quantitatively represented by OH* fluctuations, OH* does reliably capture the spatiotemporal characteristics of the subsystem [25]. It can therefore be used to construct a consistent network.

4.4. Differences between turbulence and HRR networks

Although the vortical structures and the HRR field are interconnected and mutually interacting, the corresponding networks had vastly different properties. Both networks considered the same thermoacoustic system, yet the features of one were not mirrored in the other. Whereas the turbulence network consistently exhibited power law in the degree distribution, the HRR correlation network did not appear to follow any of the candidate probability distributions. In the absence of power law, the HRR correlation network did not exhibit hub structures. As an additional finding, the power law was fulfilled for the HRR correlation network only when considering the link strength probability distribution. The presence of power law among the connections rather than nodes is unlikely to be coincidental.

Moreover, while the HRR correlation network was evolving rapidly with time and between different dynamical states, the turbulence network was much more permanent. For certain parameters, significant changes in the HRR network were not reflected in the turbulence network. The former responded to changes of the fuel composition throughout, whereas the latter did only so in the lower HFF range. Overall, one could expect that increasing HFF at a constant thermal load and equivalence ratio would significantly affect the flowfield, mixing and hydrodynamics of the system. However, for HFF values above 40%, no major changes were observed in the turbulence network and its hubs structure, after the flowfield switched to wider swirl branches. Below the threshold no significant flowfield alterations could be consistently linked to one of the turbulence network properties. With the hubs structures not changing, neither did the overall behavior of the network,

Table 2: Summary of encountered network properties and linked to their corresponding network theory and proposed physical interpretation or consequences.

Network	Observation	Network Theory	Physical Interpretation
Turbulence	Power law distribution	Great disproportion between nodes in strength and number	Vortical effects mostly minor; a few extreme exceptions
	Hub presence	Network prone to targeted node removal	Presence of a region critical for instability driving
	Exponent $\gamma < 4$	Small world property	Flowfield reacts globally to local velocity perturbations
	Exponent $\gamma > 3$ $\forall$ HFF $> 0\%$	Network is not scale-free	Fuel blend inhomogeneity introduces different scales
HRR	Mean degree $\langle \bar{k} \rangle$ varies with HFF	Network connectivity sensitive to HFF	Synchronization of the HRR field changes with HFF
	Mean degree $\langle k \rangle(t)$ varies with time	Network connectivity time-dependent	Synchronization of the HRR field changes with p'_{rms}

which we believe to be a important finding in itself. In the high HFF range, the reactive field was more sensitive to fuel composition changes than the vortical structures as reflected by the HRR and turbulence networks, respectively.

Considering temporal variations, only the HRR correlation network measures exhibited substantial fluctuations. Those were in fact well related to p'_{rms}. On the other hand, the turbulence network did not display significant temporal patterns. The HRR correlation network contained therefore more information on pressure oscillations and would be better suited to prediction of the amplitude of the limit cycle.

Overall, the introduction of hydrogen fuel did not challenge previous results of the complex network theory in thermoacoustics. The turbulent networks still exhibited power law and small world property as well as hub structures [7, 15]. The thermoacoustic instability was associated with more coherent networks [14], here an HRR one.

4.5. Physical interpretation of the network properties

Interpretation of the results of complex network analysis is often not immediately clear. Drawing physical insight into combustion and fluid dynamics from the network properties is a well-established challenge and an ongoing field of research [9]. In Table 2 we present interpretations which are well established in complex network theory as well as our own proposed physical interpretations of the results.

5. Summary and Conclusions

We constructed turbulence and heat release rate networks to understand the effects of vortical structures and coherent heat release rate oscillations, respectively, in the hydrogen-enriched PRECCINSTA burner. Such a two-pronged network analysis is performed for the first time in the combustion literature. Turbulence networks exhibited power law degree distribution throughout the whole range of dynamical states and hydrogen enrichment as well as consistently retained the 'small world' property, signifying quick information propagation and global influence of local perturbations. Moreover, it was confirmed that vortical structures resulted in a turbulence network featuring hubs, that were present and remained stationary throughout all HFFs tested. Any previously developed turbulence hub suppression techniques would remain valid for those mixtures and would not require target location adjustments.

Increasingly coherent oscillations of the heat release rate field identified by denser HRR networks coincided with shifts towards dynamical instability. Pearson correlation provided connections more robust and sensitive to changes in dynamical state than other dependence measures, while being simpler and more efficient. Yet, the time-averaged quantities suggested that correlation levels on their own were insufficient to quantify the resultant overall p'_{rms}. However, the evolution of the HRR correlation network reflected well the changes in p'_{rms}. The cross-correlation between the signals preserved high positive values. Additionally, the associated time-delay indicated that the mean degree $\langle k \rangle$ of the heat release network usually preceded the changes in p'_{rms}.

The results from this study show that turbulence and HRR networks, despite being constructed for the same thermoacoustic system, can have vastly different properties.

Acknowledgments

This work is part of the Marie Skłodowska-Curie Innovative Training Network Pollution Know-How and Abatement (POLKA). We gratefully acknowledge the financial support from the European Unions under the Horizon 2020 Marie Skłodowska-Curie grant agreement No. 813367. This project has

also received funding from the European Research Council (ERC) under Horizon 2020 Grant Agreement No. 682383. Sujith gratefully acknowledges funding from the IoE initiative of IIT Madras (SB/2021/0845/AE/MHRD/002696).

References

[1] T. Lieuwen, V. Yang (Eds.), Combustion Instabilities in Gas Turbine Engines: Operational Experience, Fundamental Mechanisms and Modeling, no. v. 210 in Progress in Astronautics and Aeronautics, American Institute of Aeronautics and Astronautics, Reston, VA, 2005.

[2] J. W. S. Rayleigh, The explanation of certain acoustical phenomena, Nature 18 (1878) 319–321.

[3] M. Bothien, P. Breuhaus, P. Griebel, B. Kaplan, G. Laagland, P. Stuttaford, Hydrogen gas turbines–the path towards a zero-carbon gas turbine, ETN Global (2020) 2.

[4] R. W. Schefer, C. White, J. Keller, Lean Hydrogen Combustion, in: Lean Combustion, Elsevier, 2008, pp. 213–253. doi:10.1016/B978-012370619-5.50009-1.

[5] A. Kushwaha, P. Kasthuri, S. A. Pawar, R. I. Sujith, I. Chterev, I. Boxx, Dynamical Characterization of Thermoacoustic Oscillations in a Hydrogen-Enriched Partially Premixed Swirl-Stabilized Methane/Air Combustor, Journal of Engineering for Gas Turbines and Power 143 (12) (2021) 121022. doi:10.1115/1.4052091.

[6] G. Oztarlik, L. Selle, T. Poinsot, T. Schuller, Suppression of instabilities of swirled premixed flames with minimal secondary hydrogen injection, Combustion and Flame 214 (2020) 266–276. doi:10.1016/j.combustflame.2019.12.032.

[7] A. Krishnan, R. Sujith, N. Marwan, J. Kurths, Suppression of thermoacoustic instability by targeting the hubs of the turbulent networks in a bluff body stabilized combustor, Journal of Fluid Mechanics 916 (2021) A20. doi:10.1017/jfm.2021.166.

[8] A.-L. Barabási, M. Pósfai, Network Science, Cambridge University Press, Cambridge, United Kingdom, 2016.

[9] G. Iacobello, L. Ridolfi, S. Scarsoglio, A review on turbulent and vortical flow analyses via complex networks, Physica A: Statistical Mechanics and its Applications 563 (2021) 125476. doi:10.1016/j.physa.2020.125476.

[10] R. I. Sujith, V. R. Unni, Complex system approach to investigate and mitigate thermoacoustic Instability in turbulent combustors, Phys. Fluids A (2020). doi:10.1063/5.0003702.

[11] K. Calò, D. Gallo, D. A. Steinman, V. Mazzi, S. Scarsoglio, L. Ridolfi, U. Morbiducci, Spatiotemporal Hemodynamic Complexity in Carotid Arteries: An Integrated Computational Hemodynamics and Complex Networks-Based Approach, IEEE Transactions on Biomedical Engineering 67 (7) (2020) 1841–1853. doi:10.1109/TBME.2019.2949148.

[12] M. Gopalakrishnan Meena, A. G. Nair, K. Taira, Network community-based model reduction for vortical flows, Physical Review E 97 (6) (2018) 063103. doi:10.1103/PhysRevE.97.063103.

[13] T. Kobayashi, S. Murayama, T. Hachijo, H. Gotoda, Early Detection of Thermoacoustic Combustion Instability Using a Methodology Combining Complex Networks and Machine Learning, Physical Review Applied 11 (6) (2019) 064034. doi:10.1103/PhysRevApplied.11.064034.

[14] A. Krishnan, R. I. Sujith, N. Marwan, J. Kurths, On the emergence of large clusters of acoustic power sources at the onset of thermoacoustic instability in a turbulent combustor, Journal of Fluid Mechanics 874 (2019) 455–482. doi:10.1017/jfm.2019.429.

[15] S. Murayama, H. Kinugawa, I. T. Tokuda, H. Gotoda, Characterization and detection of thermoacoustic combustion oscillations based on statistical complexity and complex-network theory, Physical Review E 97 (2) (2018) 022223. doi:10.1103/PhysRevE.97.022223.

[16] A. Krishnan, R. Manikandan, P. R. Midhun, K. V. Reeja, V. R. Unni, R. I. Sujith, N. Marwan, J. Kurths, Mitigation of oscillatory instability in turbulent reactive flows: A novel approach using complex networks, EPL (Europhysics Letters) 128 (1) (2019) 14003. doi:10.1209/0295-5075/128/14003.

[17] S. Scarsoglio, G. Iacobello, L. Ridolfi, Complex Networks Unveiling Spatial Patterns in Turbulence, International Journal of Bifurcation and Chaos 26 (13) (2016) 1650223. doi:10.1142/S0218127416502230.

[18] R. G. W. A. N. M. J. K. Praveen Kasthuri, Abin Krishnan, R. I. Sujith, Investigation into the coherence of flame intensity oscillations in a model multi-element rocket combustor using complex networks, Physics of Fluids 34 (2022) 034107. doi:https://doi.org/10.1063/5.0080874.

[19] W. Meier, P. Weigand, X. Duan, R. Giezendannerthoben, Detailed characterization of the dynamics of thermoacoustic pulsations in a lean premixed swirl flame, Combustion and Flame 150 (1-2) (2007) 2–26. doi:10.1016/j.combustflame.2007.04.002.

[20] I. Chterev, I. Boxx, Effect of hydrogen enrichment on the dynamics of a lean technically premixed elevated pressure flame, Combustion and Flame 225 (2021) 149–159.

[21] K. Taira, A. G. Nair, S. L. Brunton, Network structure of two-dimensional decaying isotropic turbulence, Journal of Fluid Mechanics 795 (May 2016). doi:10.1017/jfm.2016.235.

[22] V. Nair, R. Sujith, Multifractality in combustion noise: Predicting an impending combustion instability, Journal of Fluid Mechanics 747 (2014) 635–655. doi:10.1017/jfm.2014.171.

[23] S. Shima, K. Nakamura, H. Gotoda, Y. Ohmichi, S. Matsuyama, Formation mechanism of high-frequency combustion oscillations in a model rocket engine combustor, Physics of Fluids 33 (6) (2021) 064108. doi:10.1063/5.0048785.

[24] V. Godavarthi, S. A. Pawar, V. R. Unni, R. I. Sujith, N. Marwan, J. Kurths, Coupled interaction between unsteady flame dynamics and acoustic field in a turbulent combustor, Chaos: An Interdisciplinary Journal of Nonlinear Science 28 (11) (2018) 113111. doi:10.1063/1.5052210.

[25] P. Agostinelli, D. Laera, I. Chterev, I. Boxx, L. Gicquel, T. Poinsot, On the impact of h2-enrichment on flame structure and combustion dynamics of a lean partially-premixed turbulent swirling flame, Combustion and Flame 241 (2022) 112120. doi:doi.org/10.1016/j.combustflame.2022.112120.